Impact of aleatory and epistemic uncertainties on thermal risk and production assessment: application to the hydrogenation of levulinic acid and butyl levulinate

Lujie Shi, Younes Aoues, Sébastien Leveneur

Journal of Loss Prevention in the Process Industries 89 (2024) 105317

Contents lists available at ScienceDirect

Journal of Loss Prevention in the Process Industries

journal homepage: www.elsevier.com/locate/jlp

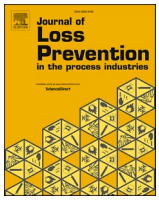

Impact of aleatory and epistemic uncertainties on thermal risk and production assessment: Application to the hydrogenation of levulinic acid and butyl levulinate

Lujie Shi [a], Younes Aoues [a], Sébastien Leveneur [b,*]

[a] INSA Rouen Normandie, Normandie Univ, LMN UR 3828, F-76000, Rouen, France
[b] INSA Rouen Normandie, Univ Rouen Normandie, Normandie Univ, LSPC UR 4704, F-76000, Rouen, France

ARTICLE INFO

Keywords:
GVL production
Thermal runaway risk
Uncertainty propagation
Global sensitivity analysis

ABSTRACT

The hydrogenation of levulinates, derivatives from cellulose hydrolysis, leads to the platform molecule γ-valerolactone (GVL). While prior investigations indicate the propensity for thermal runaways in this reaction, a comprehensive sensitivity analysis has been conspicuously absent in the existing literature. This study endeavors to scrutinize the influence of input parameters on both thermal risks and the production rate during GVL synthesis. Distinguished by its dual focus on sensitivity analyses, this manuscript also contrasts the implications of aleatory and epistemic uncertainties on thermal risk and production metrics. Aleatory uncertainties arise from the inherent variability of initial conditions, while epistemic uncertainties emanate from incomplete knowledge of the kinetic model. Employing Sobol global sensitivity analysis on the kinetic model, we delineate the hierarchical importance of various parameters. This analysis incorporates a quantification of uncertainty, and algorithmic approaches are proffered. The findings reveal that the initial temperature, the initial mass of the Ru/C catalyst, and hydrogen pressure are pivotal factors that are directly proportional to thermal risk and production efficiency. The implications of uncertainty on these variables are also discussed.

1. Introduction

Biomass is a renewable resource, and its valorization can contribute to the sustainable development of a region, reduce greenhouse gas emissions, and support a circular economy (Amjith and Bavanish, 2022; Tursi, 2019). Using biomass raw materials, which are not competing with the food sector, is vital. For that reason, lignocellulosic biomass (LCB), such as agricultural waste or short rotation coppice, should be favored. The valorization of lignocellulosic biomass is essential due to its sustainability, versatility, and economic benefits. It holds promise as a key component in the transition towards a more sustainable, circular, and bio-based economy.

LCB consists of polymers of sugars (cellulose and hemicellulose) and aromatic compounds (lignin) in different ratios according to the plant's nature, season, etc. The valorization of sugar fraction is well-developed in academia, and there are some processes at an industrial scale. The strategy favors the production of platform molecules such as levulinic acid (LA) and its levulinate, ethanol or butanol, 2,5-Furandicarboxylic acid, etc (Ashokkumar et al., 2022). Among these platform molecules, γ-valerolactone (GVL) (González and Area, 2021; Dutta et al., 2019; Lê et al., 2018), produced from the hydrogenation of levulinic acid or alkyl levulinate, is considered as a promising molecule to be used as a solvent, starting material for polymers or biofuels (Yan et al., 2015; Alonso et al., 2013; Horváth et al., 2008). One of the most efficient ways of production is the hydrogenation of levulinic acid or alkyl levulinate by molecular hydrogen over Ru/C (Wang et al., 2019). The kinetic model developed by Delgado et al. (2022) was used in this study. This model described the kinetics of levulinic acid (LA) and butyl levulinate (BL) hydrogenation into GVL over Ru/C (Delgado et al., 2023). The kinetic and thermodynamic constants obtained from Delgado et al. were used in this study.

However, this GVL production is quite exothermic (Wang et al., 2020). If the heat generated from these reactions is not properly managed, it can lead to a thermal runaway situation (Dakkoune et al., 2019). Thermal runaway is a phenomenon that occurs when a chemical reaction generates heat faster than it can be absorbed by the environment, causing the temperature to rise uncontrollably. This can lead to secondary reactions and reactor explosion due to fast pressure increase. Several studies have investigated thermal runaway in chemical

* Corresponding author.
E-mail address: sebastien.leveneur@insa-rouen.fr (S. Leveneur).

https://doi.org/10.1016/j.jlp.2024.105317
Received 27 September 2023; Received in revised form 1 March 2024; Accepted 11 April 2024
Available online 15 April 2024

processes (Kummer and Varga, 2021; Dakkoune et al., 2020; Leveneur et al., 2016). Moreover, recent research showed that 25% of major chemical plant accidents resulted from thermal runaways in France (Dakkoune et al., 2018). There are three causes: technical and physical, human and organizational, and natural causes. The human and organizational are the main causes of thermal runaway, principally operator errors. The operator errors include wrong chemical or catalyst loadings, initial temperature, feeding rates, and pressures. Hence, it is vital to determine the effect of the different input parameters on the risk of thermal runaway to implement adequate safety barriers. Generally, related research can be categorized into two main areas: uncertainty propagation and sensitivity analysis.

On the one hand, the uncertainty propagation holds a significant position in the study of chemical processes. Abdi et al., 2023a, 2023b applied error-in-variables model (EVM) methods for output estimation with the uncertain input variables. Lyagoubi et al. (2022) imposed random variations on the input parameters of a chemical reactor and studied the impact on the system reliability. Ali et al. (2018) and Duong et al. (2016) used Monte Carlo (MC) and Halton-based quasi-MC (QMC) methods to give an in-depth understanding of uncertainty propagation in the chemical process. However, these studies have solely focused on the uncertainty of initial condition parameters.

In fact, the uncertainties mainly fall into two categories (Shi et al., 2023): aleatory and epistemic uncertainty. Aleatory uncertainty arises from variability in input parameters due to natural fluctuations, such as physical limitations, measurement errors, or inherent random-ness in the process variables. While, epistemic uncertainty is related to the lack of knowledge or the incompleteness of information. It arises from the knowledge of reaction mechanisms and uncertainties from kinetic parameter estimations. To deal with both aleatory and epistemic uncertainty, several methods have been developed including probabilistic methods (such as Monte Carlo simulations (Mohammadi and Cremaschi, 2022), approximations methods (Nannapaneni and Mahadevan, 2016)) and non-probabilistic methods (such as interval analysis (Li et al., 2016), evidence theory (Tang et al., 2017), and so on). For example, Zhang et al. (2018) focused on the hybrid reliability analysis with both random and interval variables. Liu et al. (2017) employed P-box models, combining distribution and interval analysis, to deal with the uncertain-but-bounded variables. Building upon previous research, credible intervals are implied to represent epistemic uncertainty due to its expressiveness and computational simplicity in this study.

On the other hand, sensitivity analysis, especially global sensitivity analysis, serves as an outstanding tool for parameters importance assessment. For instance, Garcia-Hernandez et al. (2022) conducted a global sensitivity analysis on four thermal risk and optimization parameters using a vegetable oil epoxidation kinetic model. Martinez et al. (2022) used Sobol method to identify the main parameters in the anaerobic digester process. Nevertheless, most developed kinetic models use deterministic operating conditions, i.e., fixed initial temperature, initial concentrations, etc. These studies are carried out based on kinetic models. These kinetic models are usually obtained from experiments performed at different operating conditions. The estimated kinetic constants used in the modeling are obtained within credible intervals. The drawback of this approach is that the propagation of uncertainty/error should be included in the sensitivity analysis.

In this study, a global sensitivity analysis for GVL production with BL and LA was evaluated with considering the parameters uncertainty. A sensitivity-uncertainty analysis procedure is proposed to assess the influence of the eight initial inputs on two key output parameters: risk indicator and production rate. To the best of our knowledge, the uncertainties are not included in the sensitivity analysis. The current paper focuses majorly on: (1) An uncertainty propagation analysis considering mixed aleatory and epistemic uncertainty. (2) A Sobol sensitivity analysis with parameters' mixed uncertainty. (3) Implement of this Sobol-uncertainty sensitivity analysis on the GVL production reaction that evaluate the effect of the initial condition parameters.

The paper is organized as follows: Section 2 gives the GVL synthesis process and kinetic model and introduces inputs and outputs. Section 3 proposes a mixed uncertainty, which is calculated based on epistemic uncertainty described by interval analysis and aleatory uncertainty described by probabilistic distribution. For sensitivity analysis, the standard procedure and solution with uncertainty of Sobol method are presented in Section 4. The results of uncertainty propagation and Sobol analysis with uncertainty are shown and interpreted in Section 5. Finally, a brief conclusion and future work are given in Section 6.

2. Kinetic model and thermal risk

2.1. Chemical materials and methods

The chemical production process in this study is the production of GVL by hydrogenation of levulinic acid (LA) and butyl levulinate (BL) with the catalyst Ru/C and Amberlite IR-120 (Amb). It is a two-step reaction shown in Fig. 1. The first step is hydrogenating LA and BL to the intermediate (HPA and BHP). The second step is the cyclization of the intermediate to GVL. For a detailed introduction to the kinetic model of this production process, one could refer to the research by Delgado et al. (2022).

As the previous studies of our group (Delgado et al., 2022; Wang et al., 2020), this system is a two-step reaction comprising a hydrogenation and cyclization step, while the hydrogenation is an exothermic step (Garcia-Hernandez et al., 2019) and governs the reaction temperature.

Under normal processes, the reaction is conducted under isothermal conditions with an appropriate and efficient cooling system. In the case of cooling failure, the system can go from isothermal to adiabatic conditions (Salcedo et al., 2023). For that reason, thermal risk assessment is done in adiabatic and batch conditions, which are the most conservative, so thermal risk assessment is done in such a mode.

2.2. Kinetic model and parameters characterization

In order to analyze the GVL production process, we have identified eight input parameters that listed in Table 1. These parameters control the initial conditions for the process, and were varied in models developed by Delgado et al. (2022).

In Table 1, the input parameters are represented as $\mathbf{X} = [X_1, X_2, \cdots X_i, \cdots, X_I](I = 8)$. Concerning the inputs in Table 1, we have restricted our study to input parameters whose value in the range of lower value and higher value. In this study, aleatory uncertainty due to measurement errors or variations in parameters is represented by these parameters with normal distributions. Firstly, this assumption is grounded in empirical data obtained from previous experiments. The observed values from these experiments exhibit characteristics consistent with a normal distribution, suggesting its appropriateness for modeling. Secondly, the rationale for adopting a normal distribution is supported by literature references (Abdi et al., 2023a, 2023b; Duong et al., 2016). This reference provides theoretical and empirical justifications for the prevalence of normal distributions in similar contexts, reinforcing the validity of this assumption in our study.

In this model, 43 parameters can be divided into two parts. One part, listed as $\mathbf{M} = [M_1, M_2, \cdots M_i, \cdots, M_I](I = 18)$ in Table 2, these parameters are not known precisely, but are known to fall within certain ranges. They are described as an interval with a center, a lower and an upper bound. In this study, these intervals provide epistemic uncertainty.

The other part, listed as $\mathrm{Mf} = [Mf_1, Mf_2, \cdots Mf_i, \cdots, Mf_I](I = 25)$ in Table 3, is the constant parameters in this model. These parameters are considered deterministic.

As indicated by Delgado et al. (2022), the more reliable kinetic model is the non-competitive Langmuir-Hinshelwood kinetic model with hydrogen dissociation, where levulinate (BL and LA) and hydrogen are adsorbed on different sites. The main differential equations based on

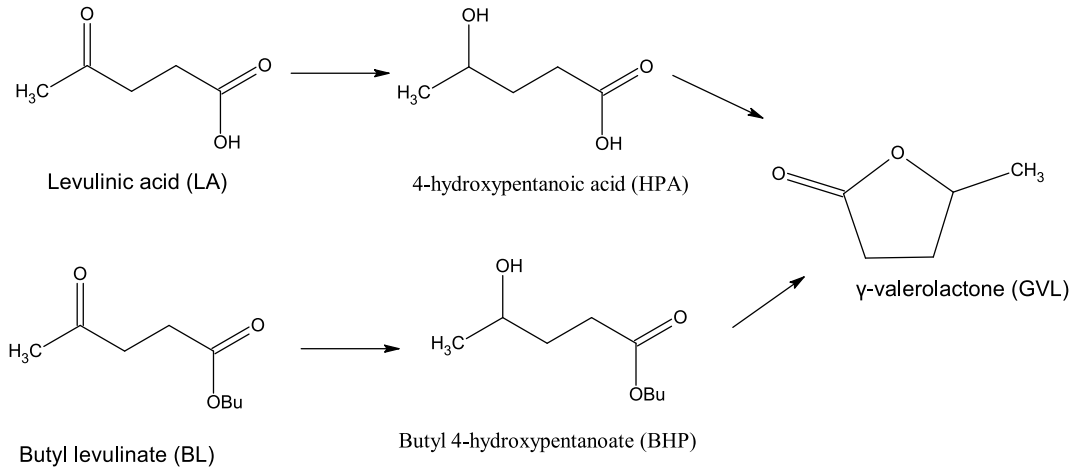

Fig. 1. Reaction steps of LA and BL to GVL over Ru/C and Amberlite IR-120.

Table 1
Variation and uncertainty of the input parameters.

No.	Parameters	lower value	higher value	3*Standard deviation	Distribution	Definition	Unit
X_1	T_{j0}	90	140	1	Normal	Initial temperature of the jacket	K
X_2	P_{H2}	20	50	2	Normal	Initial pressure of H_2	bar
X_3	UA	80	120	5	Normal	Heat transfer coefficient	W\/K
X_4	m_{LA0}	0.09	0.11	0.01	Normal	Initial mass of LA	kg
X_5	m_{BL0}	0.19	0.21	0.01	Normal	Initial mass of BL	kg
X_6	m_{GVL0}	0.09	0.11	0.01	Normal	Initial mass of GVL	kg
X_7	m_{Ru}	0.001	0.003	0.0003	Normal	Initial mass of Ru	kg
X_8	m_{Amb}	0.005	0.02	0.002	Normal	Initial mass of Amb	kg

Table 2
Kinetic model parameters with interval value.

NO.	Parameter	Center	Lower bound	Upper bound	Unit
M_1	$k_{BL\_hyd}(T_{Ref})$	3.02E-06	2.68E-06	3.36E-06	$m^3.mol^{-1}.s^{-1}.kg.dryRuC^{-1}$
M_2	Ea_{BL_hyd}	3.62E+04	3.35E+04	3.89E+04	$J.mol^{-1}$
M_3	$k'_{BHP\_cat\_Amb}(T_{Ref})$	4.36E-05	2.25E-05	6.47E-05	$s^{-1}.kg.dryAmb^{-1}$
M_4	$k_{BHP\_noncat}(T_{Ref})$	5.93E-05	4.13E-05	7.73E-05	s^{-1}
M_5	Ea_{BHP_noncat}	7.78E+04	4.99E+04	1.06E+05	$J.mol^{-1}$
M_6	$k_{LA\_hyd}(T_{Ref})$	7.75E-06	7.04E-06	8.46E-06	$m^3.mol^{-1}.s^{-1}.kg.dryRuC^{-1}$
M_7	Ea_{LA_hyd}	4.61E+04	4.31E+04	4.91E+04	$J.mol^{-1}$
M_8	K_{LA}	1.69E-03	1.42E-03	1.96E-03	$m^3.mol^{-1}$
M_9	$k'_{HPA\_cat\_Amb}(T_{Ref})$	4.79E-04	2.43E-04	7.15E-04	$s^{-1}.kg.dryAmb^{-1}$
M_{10}	$k_{HPA\_noncat}(T_{Ref})$	1.25E-06	0.00E+00	2.50E-06	s^{-1}
M_{11}	Ea_{HPA_noncat}	4.15E+05	3.15E+05	5.15E+05	$J.mol^{-1}$
M_{12}	$k_{BHP\_RuC}(T_{Ref})$	2.41E-05	1.99E-05	2.83E-05	$s^{-1}.kg.dryRuC^{-1}$
M_{13}	$k_{HPA\_RuC}(T_{Ref})$	5.74E-05	5.30E-05	6.18E-05	$s^{-1}.kg.dryRuC^{-1}$
M_{14}	Kc	1.59E-04	1.19E-04	1.99E-04	$m^3.mol^{-1}$
M_{15}	$k_{BHP\_diss}(T_{Ref})$	1.69E-06	1.42E-06	1.96E-06	$m^3.mol^{-1}.s^{-1}$
M_{16}	Ea_{BHP_diss}	1.09E+05	9.50E+04	1.23E+05	$J.mol^{-1}$
M_{17}	$k_{HPA\_diss}(T_{Ref})$	4.73E-06	4.41E-06	5.05E-06	$m^3.mol^{-1}.s^{-1}$
M_{18}	Ea_{HPA_diss}	6.70E+04	6.16E+04	7.24E+04	$J.mol^{-1}$

Table 3
Kinetic model parameters with fixed value.

No	Parameter	Value	Unit
Mf_1	T_{ref}	392.72	K
Mf_2	K_{H2}	0	$m^3.mol^{-1}$
Mf_3	K_{BL}	0	$m^3.mol^{-1}$
Mf_4	$Ea'_{BHP\_cat\_Amb}$	0	$J.mol^{-1}$
Mf_5	$Ea'_{HPA\_cat\_Amb}$	0	$J.mol^{-1}$
Mf_6	Ea_{BHP_RuC}	0	$J.mol^{-1}$
Mf_7	Ea_{HPA_RuC}	0	$J.mol^{-1}$
Mf_8	$K_{BHP-SO3H}$	0	$m^3.mol^{-1}$
Mf_9	K_{HPA}	0	$m^3.mol^{-1}$
Mf_{10}	K_{c2}	0	$m^3.mol^{-1}$
Mf_{11}	$K_{LA\_modified}$	2.22E-06	s^{-1}
Mf_{12}	R	8.314	$J.mol^{-1}.K^{-1}$
Mf_{13}	He(373K)	1.86	$mol.m^{-3}.bar^{-1}$
Mf_{14}	ΔH_{sol}	5936.8	$J.mol^{-1}$
Mf_{15}	$\Delta H_{r1,BL}$	−3.56E+04	$J.mol^{-1}$
Mf_{16}	$\Delta H_{r2,BL}$	6.40E+03	$J.mol^{-1}$
Mf_{17}	$\Delta H_{r1,LA}$	−4.97E+04	$J.mol^{-1}$
Mf_{18}	$\Delta H_{r2,LA}$	9.00E+03	$J.mol^{-1}$
Mf_{19}	M(BL)	1.72E-01	$kg.mol^{-1}$
Mf_{20}	M(BHP)	1.74E-01	$kg.mol^{-1}$
Mf_{21}	M(GVL)	1.00E-01	$kg.mol^{-1}$
Mf_{22}	M(ROH)	7.41E-02	$kg.mol^{-1}$
Mf_{23}	M(LA)	1.16E-01	$kg.mol^{-1}$
Mf_{24}	M(HPA)	1.18E-01	$kg.mol^{-1}$
Mf_{25}	M(W)	1.80E-02	$kg.mol^{-1}$

the material and energy balances in batch reactor regarding time t and energy balance can be expressed as Eq. (1).

$$
\begin{aligned}
\frac{dC_{BL}}{dt} &= -R_{BL\_hyd}\\
\frac{d[H_2]_{liq}}{dt} &= k_{la}^{*}\left([H_2]^{*}_{liq} - [H_2]_{liq}\right) - R_{BL\_hyd} - R_{LA\_hyd}\\
\frac{dC_{BHP}}{dt} &= R_{BL\_hyd} - R_{BHP\_noncat} - R_{BHP\_RuC} - R_{BHP\_SO3H} - R_{BHP\_diss}\\
\frac{dC_{BuOH}}{dt} &= R_{BHP\_noncat} + R_{BHP\_RuC} + R_{BHP\_SO3H} + R_{BHP\_diss}\\
\frac{dC_{LA}}{dt} &= -R_{LA\_hyd}\\
\frac{dC_{HPA}}{dt} &= R_{LA\_hyd} - R_{HPA\_noncat} - R_{HPA\_RuC} - R_{HPA\_SO3H} - R_{HPA\_diss}\\
\frac{dC_{water}}{dt} &= R_{BL\_hyd} - R_{HPA\_noncat} + R_{HPA\_RuC} + R_{HPA\_SO3H} + R_{HPA\_diss}\\
\frac{dC_{GVL}}{dt} &= R_{BHP\_noncat} + R_{BHP\_RuC} + R_{BHP\_SO3H} + R_{BHP\_diss} + R_{HPA\_noncat} + R_{HPA\_RuC} + R_{HPA\_SO3H} + R_{HPA\_diss}\\
&\quad \left(-R_{Hydrogenation} \bullet \Delta H_{R,Hydrogenation} \bullet V - R_{Cyclization} \bullet \Delta H_{R,Cyclization} \bullet V\right) +\\
\frac{dT_R}{dt} &= \frac{UA \bullet \left(T_j - T_R\right)}{m_R \bullet C_{PR} + m_{insert} \bullet Cp_{insert} + m_{catalyst} \bullet Cp_{catalyst}}
\end{aligned}
\tag{1}
$$

All parameters in the right of Eq. (1) are obtained by the parameters in Table 1, Tables 2 and 3. The ODEs for the mass and energy balances were solved out by using the solver "solve_ ivp" based on Backward Differentiation Formulas (BDF) (Virtanen et al., 2020). For the sake of simplicity, the kinetic model with differential equations can be expressed as:

Table 4
The responses of the kinetic model.

No	Parameter
U_1	cBL
U_2	cLA
U_3	cBHP
U_4	cHPA
U_5	cGVL
U_6	cROH
U_7	cH2
U_8	cWater
U_9	T

$$
\begin{aligned}
\mathbf{U}(t) &= f(\mathbf{X}, \mathbf{M}, \mathbf{Mf}, t)\\
\mathbf{X} &= [X_1, X_2, \cdots, X_i, \cdots, X_I]\ (I = 8)\\
\mathbf{M} &= [M_1, M_2, \cdots, M_i, \cdots, M_I] (I = 18)\\
\mathrm{Mf} &= [Mf_1, Mf_2, \cdots, Mf_i, \cdots, Mf_I] (I = 25)\\
\mathbf{U} &= [U_1, U_2, \cdots, U_i, \cdots, X_I]\ \ (I = 8)
\end{aligned}
\tag{2}
$$

where **X**, **M** and Mf consist of initial parameters (as shown in Table 1), model variable parameters (as shown in Table 2) and model fixed parameters (as shown in Table 3), respectively. $\boldsymbol{U}(t)$ are responses regarding to time t. The elements of **U** are listed in Table 4.

2.3. Two outputs from the model: risk indicator and production rate

It is essential for all chemical processes to reduce the thermal runaway risk and improve the production rate of GVL. Hence, two outputs, including risk indicator *Ri* and production rate *Pr* are proposed in this study.

2.3.1. Risk indicator

For the thermal risk assessment of this exothermic process, it should avoid high reaction temperatures that could trigger secondary reactions and avoid the fact that the reaction temperature reached its maximum value too fast. According to Table 4, U_9 represents the temperature regarding time. Hence, two parameters for the thermal runaway risk assessment are defined: temperature increment (ΔT) and time to the maximum temperature rate (*TMR*). The thermal risk parameter ΔT was

Level			Negligible	Medium	Critical	Catastrophic
	Parameter	ΔT	<50	50-200	200-400	>400
	TMR	Factor	1	2	3	4
Impossible	>100	1	1	2	3	4
Remote	50-100h	2	2	4	6	8
Seldom	24-50h	3	3	6	9	12
Occasional	8-24h	4	4	8	12	16
Probable	1-8h	5	5	10	15	20
Frequency	<1h	6	6	12	18	24

Fig. 2. Classical risk matrix for thermal runaway.

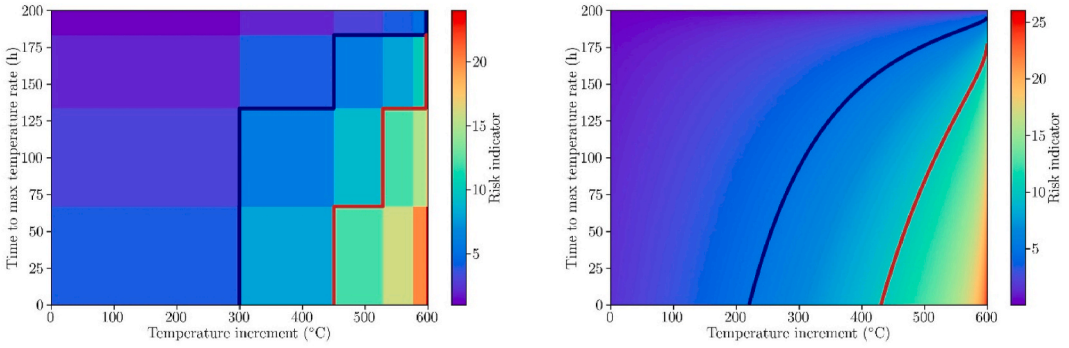

Fig. 3. Comparison of risk indicator between (a) classical risk matrix and (b) fitted method.

determined by using the developed kinetic model under adiabatic conditions in this study. The parameter ΔT is the difference between the maximum and initial reaction temperature and characterizes the severity of the risk. Moreover, *TMR* defines the time to reach the maximum temperature ratio and characterizes the probability of the thermal runaway risk.

From the literature (Stoessel, 2020; Pan et al., 2023), a risk matrix is built by ΔT and *TMR* as shown in Fig. 2.

The ΔT and *TMR* are divided by different ranges and have corresponding factors. The risk matrix's indicators are obtained by multiplying the two factors. Then, the risk indicators are divided into a non-acceptable risk zone (red), a moderate risk zone (blue), and an acceptable risk zone (green).

A drawback in this classical risk matrix is that the risk indicator can only take specific values and is not continuous. This risk matrix effectively assesses the thermal runaway risk in practice, but it may lead to numerical errors when using some statistical methods for numerical simulation. To avoid this problem, this paper applies a power function to fit the relationship between risk indicator and ΔT , *TMR* values.

$$Ri = \left(0.2449 \times (\Delta T)^{0.4372}\right) \times \left(-01.4772 \times (TMR)^{0.2894} + 7.2398\right) \quad (3)$$

In Eq. (3), two factors follow a power-law relationship with ΔT and *TMR* values separately. This fit derived from the risk matrix, which shows an exponential function passing through the origin more accurately conforms to physical laws and the trend of increasing risk. Consequently, we have defined the exponential function and the parameters are fitted using nonlinear least squares (Fig. 2).

Moreover, the final risk indicator *Ri* is also obtained by multiplying the two factors, but the values are continuous. The comparison of risk indicators between the classical risk matrix and fitted method are shown in Fig. 3.

Within the same range of values, the risk indicators in Fig. 3(b) are smoother compared to those in Fig. 3(a), without any abrupt changes. The blue lines in both figures correspond to $Ri = 5$, the boundary for the acceptable and moderate risk zones. Similarly, the red lines correspond to $Ri = 10$, which is the boundary for a moderate and non-acceptable risk zone.

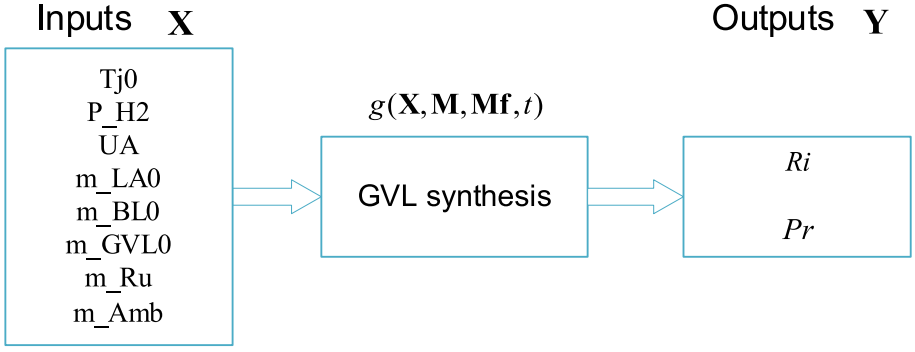

Fig. 4. Input parameters and output parameters for the GVL synthesis process.

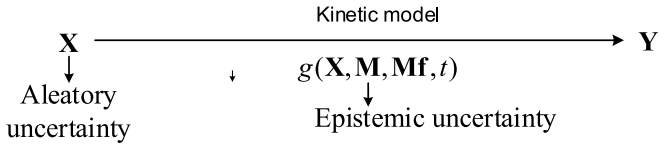

Fig. 5. Uncertainty propagation from aleatory and epistemic uncertainty.

The newly fitted risk indicator (in Eq. (3)) remains the same considerations and boundaries of risk assessment in chemical engineering processes. However, it provides more reasonable numerical values for more complex numerical analyses. It is preferable to have a low *Ri*, which can be achieved by minimizing ΔT and maximizing *TMR*.

2.3.2. Production rate

Another important point for a chemical process is economic attractiveness. According to Table 4, U_5 represents the concentration of GVL regarding time. The production rate *Pr* is defined as the ratio of the production of GVL to the time to finish the reaction. A high yield difference and short t_GVL_{final} is advantageous.

$$Pr = \frac{c\_GVL_{final} - c\_GVL_0}{t\_GVL_{final}} \tag{4}$$

In summary, these two outputs are derived from kinetic model solutions **U**. A mathematical mapping between inputs *X* and outputs *Y* is constructed as Eq. (5) and illustrated as Fig. 4.

$$\mathbf{Y} = g(\mathbf{X}, \mathbf{M}, \mathbf{Mf}, t) \tag{5}$$

In Fig. 4, eight inputs represent the initial conditions of the process, and two outputs characterize the safety and performance of the process. The sensitivity analysis in this study is based on these parameters.

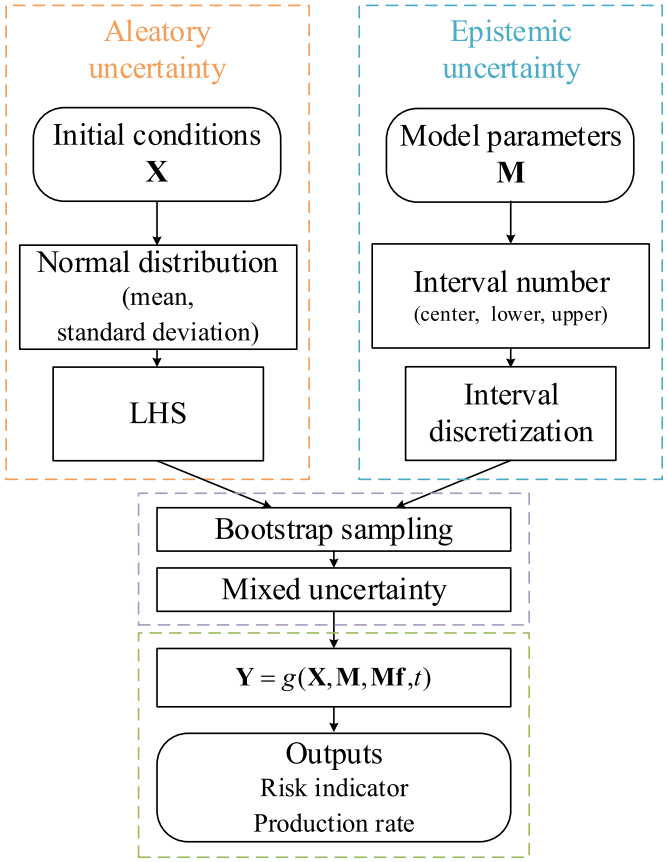

Fig. 6. Illustration of the uncertainty study method.

3. Mixed uncertainty propagation method

In fact, this process has two different sources of uncertainties, as Fig. 5 shows: aleatory un-certainty arises from initial condition parameters, and epistemic uncertainty arises from the knowledge of kinetic parameter estimations.

Considering the uncertainty, the output parameters **Y** should be a random value because of variability (aleatory uncertainty) and lack of information (epistemic uncertainty). Therefore, a mixed uncertainty propagation is proposed in this study as illustrated in Fig. 6.

As Fig. 6 shows, the mixed uncertainty includes aleatory uncertainty and epistemic uncertainty. Here, $\mathbf{X} = [X_1, X_2, \cdots X_i, \cdots, X_I]$ denotes $I = 8$ independent input parameters, and a normal distribution can describe the aleatory uncertainty. Similarly, $\mathbf{M} = [M_1, M_2, \cdots M_i, \cdots, M_J]$ denotes $J = 18$ kinetic model parameters which are described by interval number. Then the aleatory uncertainty of **X** and epistemic uncertainty of **M** lead to variable solutions **Y** by differential equations Eq. 1. Finally, these uncertainties can affect the thermal risk and production rate.

Firstly, only aleatory uncertainty is taken into account. The normal distribution is sampled by the Latin Hypercube Sampling (LHS) simulations method. 8 parameters in Table 1, used as initial conditions to the kinetic model, are represented as $\mathbf{X} = [X_1, X_2, \cdots X_i, \cdots, X_I]$ $(I = 8)$.The parameters of Table 2 are fixed to the center of the interval. The sampling number of simulations is set to *K* in this study. The sampled data are:

$$\begin{aligned} \mathbf{X} &= [X_1, X_2, \cdots X_i, \cdots, X_I] \\ X_i &= \left[x^{(1)}, x^{(2)}, \cdots, x^{(k)}, \cdots x^{(K)}\right]^{\mathrm{T}} \end{aligned} \tag{6}$$

Secondly, our analysis is confined to epistemic uncertainty. The interval analysis is used to carry out the epistemic uncertainty. Table 3 shows 18 variable parameters in the kinetic model, which are represented as $\mathbf{M} = [M_1, M_2, \cdots M_i, \cdots, M_J] (j = 18)$. In this study, the interval (M_i) could be discretized by equal width to *K* values to explore the range of plausible values due to lack of knowledge, aiming to narrow that range. Interval discrete is often appropriate, as we do not know any value within the interval to be more likely than any other. In this case, the parameters of Table 1 are fixed to the mean value of the normal distributions.

$$\begin{aligned} \mathbf{M} &= [M_1, M_2, \cdots M_i, \cdots, M_J] \\ M_i &= \left[m^{(1)}, m^{(2)}, \cdots, m^{(k)}, \cdots m^{(K)}\right]^{\mathrm{T}} \end{aligned} \tag{7}$$

Thirdly, both aleatory and epistemic uncertainties are considered. The bootstrap sampling method is used for the mixed uncertainty. The sampled points of initial conditions (aleatory uncertainty) and the interval values of the model parameters (epistemic uncertainty) are combined into the mixed uncertainty. Bootstrap sampling generates data to avoid repetition of the aleatory and epistemic uncertainty.

Bootstrap sampling is a statistical technique usually used to estimate the statistics of a population by sampling a dataset with replacement. Randomly pick one sample from each element in **X** and **M**, the re-sampled data are shown as:

$$\overline{\mathbf{X}} = \begin{bmatrix} X^{(1)} \\ \vdots \\ X^{(k)} \\ \vdots \\ X^{(K)} \end{bmatrix} = \begin{bmatrix} x_1^{(1)} & \cdots & x_i^{(1)} & \cdots & x_I^{(1)} \\ \vdots & & \vdots & & \vdots \\ x_1^{(k)} & \cdots & x_i^{(k)} & \cdots & x_I^{(k)} \\ \vdots & & \vdots & & \vdots \\ x_1^{(K)} & \cdots & x_i^{(K)} & \cdots & x_I^{(K)} \end{bmatrix} \tag{8}$$

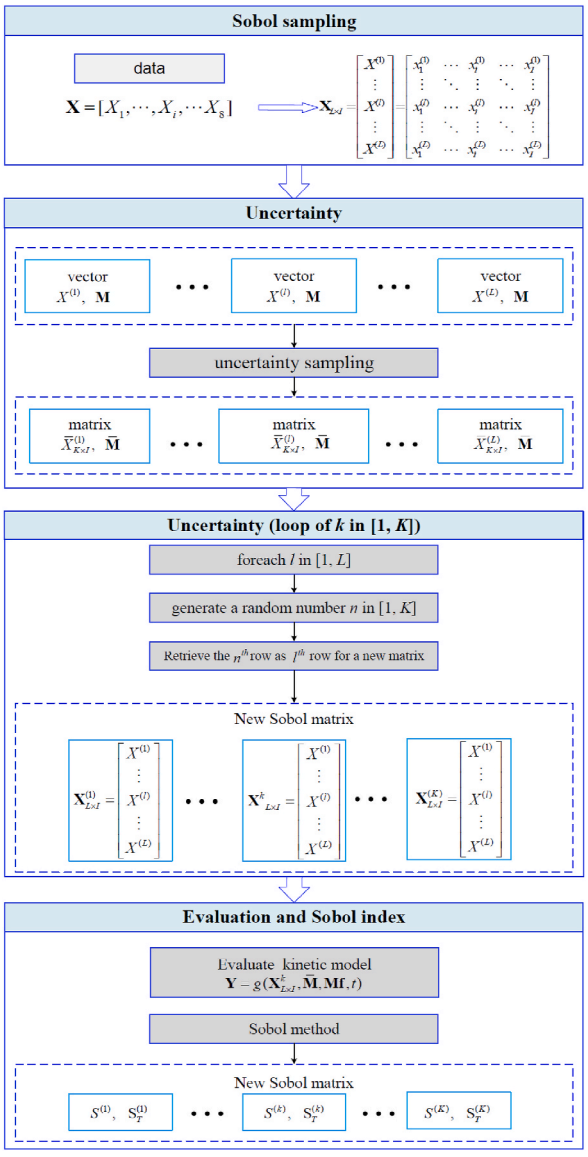

Fig. 7. Illustration of the Sobol study with uncertainty method.

$$\overline{\mathbf{M}} = \begin{bmatrix} M^{(1)} \\ \vdots \\ M^{(k)} \\ \vdots \\ M^{(K)} \end{bmatrix} = \begin{bmatrix} m_1^{(1)} & \cdots & m_j^{(1)} & \cdots & m_J^{(1)} \\ \vdots & & \vdots & & \vdots \\ m_1^{(k)} & \cdots & m_j^{(k)} & \cdots & m_J^{(k)} \\ \vdots & & \vdots & & \vdots \\ m_1^{(K)} & \cdots & m_j^{(K)} & \cdots & m_J^{(K)} \end{bmatrix} \tag{9}$$

where $\overline{\mathbf{X}}$ and $\overline{\mathbf{M}}$ is bootstrap sampled data. The subscript i,j are the ordinal number for initial parameters and model parameters, and the superscript k donates k^{th} sampling by bootstrap sampling for mixed uncertainty calculation.

The last part in Fig. 6 is evaluate the model and obtain the outputs (risk indicator and production rate) as $\mathbf{Y}$:

$$\mathbf{Y} = \begin{bmatrix} Y^{(1)} \\ \vdots \\ Y^{(k)} \\ \vdots \\ Y^{(K)} \end{bmatrix} = \begin{bmatrix} Ri^{(1)} & Pr^{(1)} \\ & \vdots \\ Ri^{(k)} & Pr^{(k)} \\ & \vdots \\ Ri^{(K)} & Pr^{(K)} \end{bmatrix} \tag{10}$$

In this study, we choose the number of bootstrap samplings is $K = 10000$, and the final sampled data are taken into Eq. (5). The uncertainty propagation including mixed uncertainty is analyzed and the results are presented in Section 5.1.

4. Sensitivity analysis with mixed uncertainty propagation method

To assess safety and efficiency in the GVL synthesis process, it is essential to conduct sensitivity analyses, considering the uncertainty associated with the parameters. Sensitivity analysis provides an understanding of how input variables affect the output variance.

The Sobol method is a global sensitivity analysis method used to decompose the variance of the output of a model into variances caused by its inputs. This method aims to understand the importance and impact of different reaction initial condition parameters and their interactions.

The statistical analysis and simulation in this section are based on inputs $\mathbf{X}$ and the outputs $\mathbf{Y}$ as listed in Fig. 1. From the kinetic model in Section 2.2, $\mathbf{X} = [X_1, X_2, \cdots X_i, \cdots, X_I]$ contains a number of I input parameters and each parameter has a finite range as listed in Table 1. $\mathbf{Y} = [Y_1, Y_2] = [Ri, Pr]$ is the output that is sensitive to the input parameters. Due to the same procedures for Ri and Pr, we focus on a single output Y to simplify the method description in this section.

4.1. Sobol global sensitivity analysis

In order to investigate the influence of different inputs for Ri and Pr, the classical Sobol method procedure is introduced in this section. Its implementation is briefly given as follows:

Step 1. Model sampling and evaluation

The first step is generating sample matrices using the Quasi-Monte Carlo (QMC) method (Tsvetkova and Ouarda, 2021). For each sampled set of inputs, compute the model to obtain the corresponding output values. Let L donate sampling number, there are input matrix with size $L \times I$ and corresponding one output Y with size L.

Based on this kinetic model, the input can be sampled by Sobol method as matrix $\mathbf{X}_{L\times I}$ and obtain the output $\mathbf{Y}_{L\times 1}$:

$$\boldsymbol{X}_{L\times I} = \begin{bmatrix} X^{(1)} \\ \vdots \\ X^{(l)} \\ \vdots \\ X^{(L)} \end{bmatrix} = \begin{bmatrix} x_1^{(1)} & \cdots & x_i^{(1)} & \cdots & x_I^{(1)} \\ \vdots & & \vdots & & \vdots \\ x_1^{(l)} & \cdots & x_i^{(l)} & \cdots & x_I^{(l)} \\ \vdots & & \vdots & & \vdots \\ x_1^{(L)} & \cdots & x_i^{(L)} & \cdots & x_I^{(L)} \end{bmatrix} \tag{11}$$

$$\boldsymbol{Y}_{L\times 2} = \begin{bmatrix} Y^{(1)} \\ \vdots \\ Y^{(l)} \\ \vdots \\ Y^{(L)} \end{bmatrix} \tag{12}$$

where $\boldsymbol{X}_{L\times I}$ and $\boldsymbol{Y}_{L\times 2}$ donate matrix from Sobol sampling that contains sampled values x and corresponding results Y. The subscript i is the ordinal number of input parameters, and the superscript l donates l^{th} sampling by Sobol method. This study selects the total sample size as $L = 4608$ (Iwanaga et al., 2022).

Step 2. Model decomposition

The key step of the Sobol method is to decompose the model $g(\mathbf{X})$ as a sum of functions of its input parameters $\mathbf{X}$. For each output Y, the model can be expressed as:

$$\begin{aligned} Y = g(\mathbf{X}) &= g_0 + \sum_{i=1}^{I} g_i(X_i) + \sum_{i<j}^{I} g_{ij}(X_i,\ X_j) + \cdots + g_{1,2,\cdots,I}(X_1, X_2, \cdots, X_I) \\ g_0 &= \mathrm{E}[Y] \\ g_i &= \mathrm{E}[Y|X_i] - g_0 \\ g_{ij} &= \mathrm{E}\left[Y|X_i,\ X_j\right] - g_0 - g_i - g_j \end{aligned} \tag{13}$$

where $\mathrm{E}(Y)$ and $\mathrm{E}(Y|X_i)$ are expectation and condition expectation respectively. Here, j is the same as i as an ordinal number and i is restricted to be less than j to avoid redundant computations.

The Sobol method's main idea is to quantify how much of the variance in the model's output is due to each of these terms. Subsequently, the variance of one output $\mathrm{V}(Y)$ can be expressed as:

$$\begin{aligned} \mathrm{V}(Y) &= \sum_{i=1}^{I} \mathrm{V}_i + \sum_{i<j}^{I} \mathrm{V}_{ij} + \cdots + \mathrm{V}_{1,2,\cdots,I} \\ \mathrm{V}_i &= \mathrm{V}[g_i(X_i)] = \mathrm{V}[\mathrm{E}(Y|X_i)] \\ \mathrm{V}_{ij} &= \mathrm{V}\left[g_{ij}(X_i, X_j)\right] = \mathrm{V}\left[\mathrm{E}(Y|X_i, X_j)\right] - \mathrm{V}_i - \mathrm{V}_j \end{aligned} \tag{14}$$

where V_i is the variance due to the i^{th} input alone and V_{ij} is the variance due to the interaction of the i^{th} and j^{th} inputs.

Step 3. Sobol index

The decomposition allows for the separation of the contributions of individual parameters and their interactions with the total output variance. Two kinds of Sobol index are used to the first-order sensitivity index S_i, which represents the proportion of the total output variance that is due to the i^{th} parameter alone:

$$S_i = \frac{\mathrm{V}(\mathrm{E}(Y|X_i))}{\mathrm{V}(Y)} = \frac{\mathrm{V}_i}{\mathrm{V}(Y)} \tag{15}$$

Furthermore, the total sensitivity index S_{Ti} captures the combined effect of the i^{th} parameter and its interactions with all other parameters:

$$S_{Ti} = \frac{\mathrm{V}(\mathrm{E}(Y|X_{\sim i}))}{\mathrm{V}(Y)} = \frac{\mathrm{V}_i}{\mathrm{V}(Y)} \tag{16}$$

where $X_{\sim i}$ donate all elements in $\mathbf{X}$ except X_i.

The first-order index quantifies the proportion of the variance in the output due to the variance in a single input parameter, ignoring all interactions with other input parameters. In comparison, the total index quantifies the proportion of the variance in the output caused by a specific input parameter, including its first-order effects and all interactions with other parameters.

4.2. Sobol method with uncertainty

Based on the standard Sobol method (in Section 4.1) and uncertainty propagation method (in Section 3), a sensitivity analysis with mixed uncertainty is proposed in this study as illustrated in Fig. 7.

Firstly, the input parameters $\mathbf{X} = [X_1, X_2, \cdots X_i, \cdots, X_I]$ can be sampled by Sobol method as matrix $\mathbf{X}_{L\times I}$ in Eq. (11). Again, $X^{(L)}$ donates l^{th} Sobol sampling for $\mathbf{X}$.

Secondly, the sampled input parameter $X^{(l)}$ and kinetic model parameter $\mathbf{M}$ are put into uncertainty analysis. As the mixed uncertainty procedure in Section 3, the input and model parameters are re-sampled as Eq. (8) and Eq. (9).

Thirdly, the number of samples in uncertainty analysis can be defined as K, and the corresponding ordinal number is k. It generates a random number n between 1 and K. Retrieve the n^{th} row from $X^{(l)}$ as l^{th} row to create a new "Sobol sampled" $X^{(k)}_{L\times I}$. Repeat the above steps with the ordinal number l until $l = L$.

Fourthly, the Sobol index with respect to input parameters is calculated. For kth calculation, we have a corresponding Sobol index $S^{(k)}$ and $S_T^{(k)}$. Repeat the blow steps with the ordinal number k. Repeat the blow steps with the ordinal number k until $k = K$. In the end, a total number of K Sobol index is obtained that contains uncertainty information.

To sum up, the peuso-code for the Sobol method with uncertainty can be listed as Algorithm 1.

Data	The input parameters: $\mathbf{X} = [X_1, X_2, \cdots, X_i, \cdots, X_I]$, and their uncertainties.
	The sampling number for Sobol method: L.
	The sampling number for uncertainty: K.
1	foreach k in $1 - K$ do (Sobol sampling for **X)**
2	foreach l in $[1, L]$ do
3	Extract $X^{(l)}$ from $\mathbf{X}_{L\times I}$
4	Put $X^{(l)}$ and M into uncertainty method
5	Obtain bootstrap sampled $\overline{\mathbf{X}}$ and $\overline{\mathbf{M}}$
6	Generate a random number n between 1 and K
7	Retrieve the n^{th} row from $\overline{\mathbf{X}}$ as l^{th} row for a new $\mathbf{X}$
8	end
9	Evaluate model by $\mathbf{Y} = g\left(\mathbf{X}, \overline{\mathbf{M}}, \mathbf{Mf}, t\right)$
10	Calculate Sobol index : $S^{(k)}$and $S_T^{(k)}$ from $\mathbf{X}$ and $\mathbf{Y}$
11	end
Results	get all Sobol index results

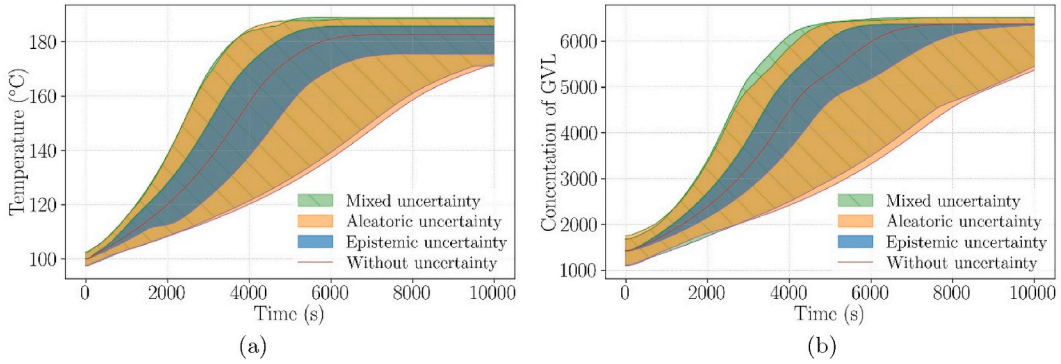

Fig. 8. Uncertainty range of (a) temperature and (b) concentration of GVL during the process.

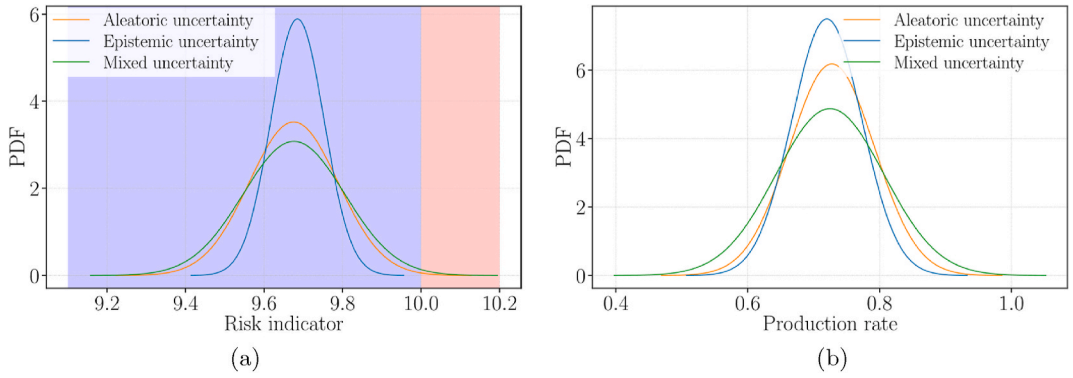

Fig. 9. PDF of (a) risk indicator and (b) production rate from uncertainty.

Table 5
Distribution parameters from uncertainty analysis.

Cases	Adiabatic						Isothermal					
Outputs	Risk indicator			Production rate			Risk indicator			Production rate		
Distribution	μ	σ	CV	μ	σ	CV	μ	σ	CV	μ	σ	CV
Aleatory uncertainty	9.68	1.13E-1	1.17E-2	7.28E-1	6.45E-2	8.89E-2	5.07E-1	3.02E-2	5.96E-2	4.59E-1	3.09E-2	6.73E-2
Epistemic uncertainty	9.69	0.68E-1	0.70E-2	7.20E-1	5.32E-2	7.39E-2	5.10E-1	1.47E-2	2.88E-2	4.61E-1	1.55E-2	3.35E-2
Mixed uncertainty	9.68	1.30E-1	1.34E-2	7.25E-1	8.18E-2	11.28E-2	5.08E-1	3.35E-2	6.6E-2	4.58E-2	3.42E-2	7.46E-2

μ: Mean, σ: Standard deviation, CV: Coefficient of Variation.

5. Results and discussions

As introduced in Section 2, the reactions occur in a reactor at the given initial conditions, and the given model is for simulating this GVL reaction process. The simulation results of uncertainty and sensitivity analysis are presented in this section.

In this section, the results are simulated and compared in adiabatic conditions (the cooling system does not work at the beginning) and

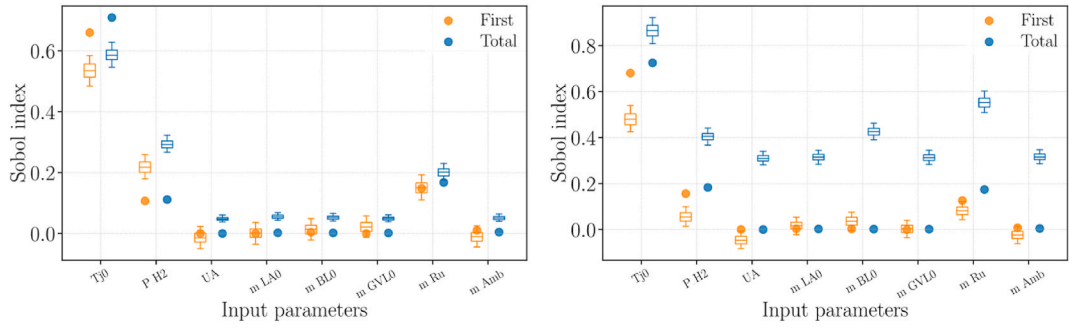

Fig. 10. Sensitivity analysis for (a) risk indicator (b) production rate under adiabatic conditions.

isothermal conditions (the reaction works with an additional cooling system).

5.1. Uncertainty propagation results

As introduced in Section 3, the uncertainty propagation is simulated for this GVL synthesis process under adiabatic conditions. The different equations calculate the reactor's temperature over time, as well as the concentrations of different compounds and other results. Two important parameters, temperature and the concentration of GVL over time, are listed in Fig. 8(a) and (b), respectively.

In Fig. 8, the red line presents the evolution of the temperature regarding time without consideration of the parameters' uncertainty. The deterministic analysis considers only the initial parameters are set to their mean values, while the model parameters are chosen to be at their center values. The center value of the interval numbers of the parameters in Table 2 and the mean values of the parameters of Table 1.

The aleatory, epistemic, and mixed uncertainty simulation results are presented in orange, blue, and green areas, respectively. The blue area is surrounded by the orange area, which means the epistemic uncertainty has a smaller dispersion than the aleatory uncertainty in our case. The green area, which is the largest one, represents mixed uncertainty. As we can see from these two figures, aleatory uncertainty occupies a dominant sensitivity for the two risk parameters.

According to the evolution of temperature and concentration of GVL, the probability density function (PDF) of the model outputs risk indicator and production rate are presented in Fig. 9.

In Fig. 9(a), the PDF of the risk indicator has less dispersion when only epistemic uncertain-ties are considered. In comparison, its PDF is scattered for aleatory and mixed uncertainty. That is, the PDFs are very close for mixed and aleatory uncertainty. These results show that the initial operating conditions parameters are more sensitive for the kinetic model for risk assessment. Moreover, Fig. 9(a) contains a moderate zone (blue background) and a non-acceptable zone (red background). The distributions of the risk indicators are mainly in the moderate zone, but in terms of the overall value, they are already nearing the non-acceptable zone. This adiabatic case shows that the production of GVL is very risky when the cooling system is stopped or fails.

In Fig. 9(b), different uncertainties lead to different PDFs for production rate. As we move from the blue and orange curve to the green curve, there is a noticeable increase in the spread of the distributions. That is, the PDF comes from mixed uncertainty is the most spread out, illustrating the highest variance among the three. These results show that both initial operating conditions and model parameters are sensitive to the production rate.

In addition, this study is also simulated under isothermal conditions. In order to compare the effect of the uncertainty, the mean values (μ), the standard deviation (σ), and the coefficient of variation of the distributions from two conditions are listed in Table 5.

Table 6
The responses of the kinetic model.

Outputs	Importance
R_i	T_{j0} m_{Ru} P_{H2}
P_r	T_{j0} m_{Ru} P_{H2}

Under adiabatic conditions, each output has almost the same mean value. Nevertheless, the standard deviation from epistemic uncertainty is much lower than others for risk indicators. In contrast, the standard deviation from aleatory uncertainty is lower than mixed uncertainty by a small difference. It is enough only to consider variations in the initial conditions (aleatory uncertainty) for the thermal risk assessment.

However, the σ value indicates that aleatory and epistemic uncertainty have similar effects on production rate. It can be seen that the CV values of the production rate are larger than that of the risk indicator, which means the parameter uncertainty has a greater impact on the production rate than thermal risk generally. If we see the isothermal condition, the risk indicators are very low, which is reasonable because if the cooling system is functioning properly, thermal runaway failure will not occur. Compared to the adiabatic, the production rate under isothermal conditions has lower μ, σ, and CV values. The low temperature decreases the production rate as well as the effect of uncertainty.

To sum up, it is necessary to consider uncertainties from both initial conditions and kinetic model parameters in assessing the thermal risk and production rate.

5.2. Sensitivity analysis with uncertainty

Following the study method in Section 4.2, the evaluation of risk indicator and production rate with respect to each input can be obtained.

The Sobol index concerning two outputs (*Ri* and *Pr*) under adiabatic and isothermal conditions are depicted in Figs. 10 and 11 respectively. Sobol index S and S_T with a number of k are shown by boxplots, k is the number of uncertainty sampling. In each boxplot, that is each input parameter, the 95th, 75th, 50th, 25th, 5th percentile values are listed.

In Figs. 10 and 11, the y-axis is the Sobol index including S (orange color) and S_T (blue color), the x-axis is eight input parameters. The deterministic Sobol indexes are represented as circles, while the Sobol indexes with uncertainty are represented as boxplots.

Figs. 10 and 11 present first-order sensitivity index and total sensitivity index. According to the total indexes, the first three most important inputs, as listed in Table 6 are initial temperature (T_{j0}), the initial concentration of catalyst Ru/C (m_{Ru}) and the initial pressure of hydrogen (P_{H2}).

Generally, the Sobol index observed in the case without uncertainty and the case with uncertainty follow a consistent trend. Three parameters, T_{j0}, m_{Ru} and P_{H2}, have the greatest effect on the outputs R_i and P_r.

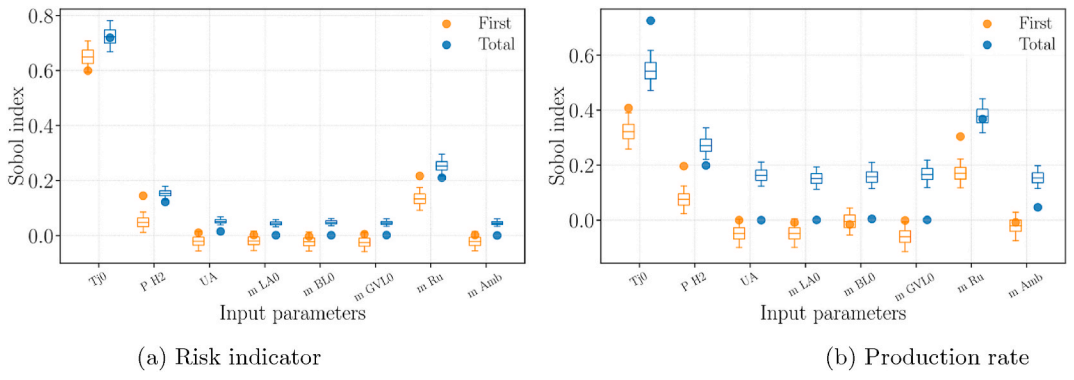

Fig. 11. Sensitivity analysis for (a) risk indicator (b) production rate under isothermal conditions.

This is consistent across all scenarios considered, with and without uncertainty, under both adiabatic and isothermal conditions. The parameters with high Sobol index significantly influence outputs, and their distribution information should be known accurately. In contrast, parameters with low Sobol index can be assumed to be deterministic variables since their contributions to the overall output are insignificant.

However, the main difference between total order Sobol index with and without uncertainty lies in the other parameters, including UA, m_{LA0}, m_{BL0}, m_{GVL0}, m_{Amb}. This disparity is particularly pronounced in terms of the production rate. As can be seen from Figs. 10(b) and Fig. 11 (b), when considering uncertainty, the total order Sobol index is not no longer zero, and the discrepancy is substantial. It also suggests that the influence of parameter uncertainties is more heavily on production rate than thermal risk.

By comparing the results with (boxplots) and without uncertainty (circles) in Figs. 10 and 11, the total-order Sobol indices (S_T) is greater than 1 when taking into account the uncertainty. It typically indicates that the input parameters interact in a way that collectively impacts the output, especially for the production rate. In this situation, changing one parameter not only directly affects the output but also changes how other parameters affect the output.

This could be an indicator that the model of GVL production is complex, with interconnected parameters that do not have simple, additive effects on the output. It suggests that to fully understand the model's behavior and to look beyond the individual contributions of each parameter in practice.

Lastly, this sensitivity procedure includes generating a sampling matrix by the Monte-Carlo method. We ran the proposed approach 5 times with varying seed quantities to mitigate the potential influence of the number of seeds. All 5 runs converge to the same result, indicating the effectiveness of the proposed method and that the results are independent of the random sampling.

6. Conclusions

The valorization of lignocellulosic biomass is rising, and exothermic hydrogenation reactions play a pivotal role in this context. Focusing on the production of γ-valerolactone (GVL) via hydrogenation of levulinic acid (LA) and butyric acid (BL) over Ru/C and Amberlite IR- 120 catalysts, this study demonstrates the influence of inputs considering the propagation of uncertainty in kinetic model responses as risk indicator and production rate.

Based on Delgado et al.' study (Delgado et al., 2022), a numerical model comprising differential equations derived from mass and energy balances is introduced. The model incorporates eight input parameters that govern the initial conditions for this chemical process. In order to measure thermal risk, an improved risk indicator is developed as one of the model outputs.

The primary objective is to examine how these initial parameters influence thermal risk and production rate output variables in GVL synthesis. To achieve this, the study conducts a sensitivity analysis of thermal runaway risk and production rate in the GVL production process while accounting for uncertainty propagation. Initially, interval analysis is employed to model epistemic uncertainty, and a normal probability distribution is used for aleatory uncertainty. Monte Carlo simulations and bootstrap sampling techniques are applied for these uncertain-ties. The findings indicate that aleatory uncertainty predominates in influencing thermal risk, whereas both aleatory and epistemic uncertainties significantly affect the production rate.

Subsequently, a global sensitivity analysis was used to find explicit relationships between eight input parameters and two output parameters. The Sobol method is implemented within a kinetic model that considers mixed uncertainties. Simulations under both adiabatic and isothermal conditions reveal that initial temperature, initial concentration of the Ru/C catalyst, and initial hydrogen pressure are the most influential parameters on both thermal risk and production rate. Furthermore, the results indicate complex interactions between the input parameters with uncertainty.

In summary, this study contributes a sensitivity methodology for risk analysis for lignocellulosic biomass valorization, ensuring safer and more efficient processes. It offers valuable insights into the sensitivity of input parameters on thermal risk and production rate while considering mixed uncertainties. This assessment could serve as a guideline for prioritizing the safety barriers in GVL production processes.

The impact of these two uncertainties is significant from the production and thermal risk standpoint. A further step can be to consider the whole process, including pretreatment and separation steps, to evaluate their impact on the cost, risk and environmental assessment. This stage is fundamental to finding the optimal operating conditions.

Nomenclature

Mf	Fixed parameters in kinetic model
M	Variable parameters in kinetic model
U	Solutions for kinetic equations
X	Input parameters
Y	Output parameters
$\mathrm{E}(\cdot)$	Expectation
$\mathrm{V}(\cdot)$	Variance
c	Concentration
Pr	Production rate
Ri	Risk indicator
S	First order of Sobol index
S_T	Total order of Sobol index
T	Temperature
t	Time (s)
Subscript	
i,j	Ordinal number of parameters
Superscript	
(l)	Ordinal number of sampling in uncertainty analysis
(k)	Ordinal number of sampling in sensitivity analysis
Glossary	
Amb	Amberlite IR-120
BHP	Butyl 4-hydroxypentanoate
BL	Butyl levulinate
GVL	γ-valerolactone
HPA	4-hydroxypentanoic acid
LA	Levulinic acid
LCB	Lignocellulosic biomass
ODE	Ordinary differential equation
PDF	Probability distribution function
Ru/C	Ruthenium on activated carbon

CRediT authorship contribution statement

Lujie Shi: Conceptualization, Data curation, Methodology, Software, Writing – original draft, Writing – review & editing. **Younes Aoues:** Conceptualization, Funding acquisition, Methodology, Software, Supervision, Writing – original draft, Writing – review & editing. **Sébastien Leveneur:** Conceptualization, Funding acquisition, Methodology, Software, Writing – original draft, Writing – review & editing.

Declaration of competing interest

The authors declare that they have no known competing financial interests or personal relationships that could have appeared to influence the work reported in this paper.

Data availability

Data will be made available on request.

Acknowledgments

This study was carried out in the framework of the ARBRE project (Risk Analysis to processes valorizing 2nd generation biomass and using

Renewable energies), which is cofounded by Euro-pean Union through the European Regional Development Fund (00130305) and by Normandy Region (21E05304).

References

Abdi, K., Celse, B., McAuley, K., 2023a. Propagating input uncertainties into parameter uncertainties and model prediction uncertainties—a review. Can J Chem Eng cjce 25015. https://doi.org/10.1002/cjce.25015.

Abdi, K., Celse, B., McAuley, K.B., 2023b. Parameter estimation and prediction uncertainties for multi-response kinetic models with uncertain inputs. AIChE J. 69, e18058 https://doi.org/10.1002/aic.18058.

Ali, W., Duong, P.L.T., Khan, M.S., Getu, M., Lee, M., 2018. Measuring the reliability of a natural gas refrigeration plant: uncertainty propagation and quantification with polynomial chaos expansion based sensitivity analysis. Reliab. Eng. Syst. Saf. 172, 103–117. https://doi.org/10.1016/j.ress.2017.12.009.

Alonso, D.M., Wettstein, S.G., Dumesic, J.A., 2013. Gamma-valerolactone, a sustainable platform molecule derived from lignocellulosic biomass. Green Chem. 15, 584. https://doi.org/10.1039/c3gc37065h.

Amjith, L., Bavanish, B., 2022. A review on biomass and wind as renewable energy for sustainable environment. Chemosphere 293, 133579. https://doi.org/10.1016/j.chemosphere.2022.133579.

Ashokkumar, V., Venkatkarthick, R., Jayashree, S., Chuetor, S., Dharmaraj, S., Kumar, G., Chen, W.-H., Ngamcharussrivichai, C., 2022. Recent advances in lignocellulosic biomass for biofuels and value-added bioproducts - a critical review. Bioresour. Technol. 344, 126195 https://doi.org/10.1016/j.biortech.2021.126195.

Dakkoune, A., Vernières-Hassimi, L., Lefebvre, D., Estel, L., 2020. Early detection and diagnosis of thermal runaway reactions using model-based approaches in batch reactors. Comput. Chem. Eng. 140, 106908 https://doi.org/10.1016/j.compchemeng.2020.106908.

Dakkoune, A., Vernières-Hassimi, L., Leveneur, S., Lefebvre, D., Estel, L., 2019. Analysis of thermal runaway events in French chemical industry. J. Loss Prev. Process. Ind. 62, 103938 https://doi.org/10.1016/j.jlp.2019.103938.

Dakkoune, A., Vernières-Hassimi, L., Leveneur, S., Lefebvre, D., Estel, L., 2018. Risk analysis of French chemical industry. Saf. Sci. 105, 77–85. https://doi.org/10.1016/j.ssci.2018.02.003.

Delgado, J., Vasquez Salcedo, W.N., Bronzetti, G., Casson Moreno, V., Mignot, M., Legros, J., Held, C., Grénman, H., Leveneur, S., 2022. Kinetic model assessment for the synthesis of gamma-valerolactone from n-butyl levulinate and levulinic acid hydrogenation over the synergy effect of dual catalysts Ru/C and Amberlite IR-120. Chem. Eng. J. 430, 133053 https://doi.org/10.1016/j.cej.2021.133053.

Delgado, J., Vásquez Salcedo, W.N., Devouge-Boyer, C., Hebert, J.-P., Legros, J., Renou, B., Held, C., Grenman, H., Leveneur, S., 2023. Reaction enthalpies for the hydrogenation of alkyl levulinates and levulinic acid on Ru/C– influence of experimental conditions and alkyl chain length. Process Saf. Environ. Protect. 171, 289–298. https://doi.org/10.1016/j.psep.2023.01.025.

Duong, P.L.T., Ali, W., Kwok, E., Lee, M., 2016. Uncertainty quantification and global sensitivity analysis of complex chemical process using a generalized polynomial chaos approach. Comput. Chem. Eng. 90, 23–30. https://doi.org/10.1016/j.compchemeng.2016.03.020.

Dutta, S., Yu, I.K.M., Tsang, D.C.W., Ng, Y.H., Ok, Y.S., Sherwood, J., Clark, J.H., 2019. Green synthesis of gamma-valerolactone (GVL) through hydrogenation of biomass-derived levulinic acid using non-noble metal catalysts: a critical review. Chem. Eng. J. 372, 992–1006. https://doi.org/10.1016/j.cej.2019.04.199.

Garcia-Hernandez, E.A., Elmoukrie, M.E., Leveneur, S., Gourich, B., Vernieres-Hassimi, L., 2022. Global sensitivity analysis to identify influential model input on thermal risk parameters: to cottonseed oil epoxidation. J. Loss Prev. Process. Ind. 77, 104795 https://doi.org/10.1016/j.jlp.2022.104795.

Garcia-Hernandez, E.A., Souza, C.R., Vernières-Hassimi, L., Leveneur, S., 2019. Kinetic modeling using temperature as an on-line measurement: application to the hydrolysis of acetic anhydride, a revisited kinetic model. Thermochim. Acta 682, 178409. https://doi.org/10.1016/j.tca.2019.178409.

González, G., Area, M.C., 2021. An overview of the obtaining of biomass-derived Gamma-valerolactone from Levulinic Acid or Esters without H2 supply. Bioresources 16, 8417–8444.

Horváth, I.T., Mehdi, H., Fábos, V., Boda, L., Mika, L.T., 2008. Gamma-valerolactone a sustainable liquid for energy and carbon-based chemicals. Green Chem. 10, 238–242. https://doi.org/10.1039/B712863K.

Iwanaga, T., Usher, W., Herman, J., 2022. Toward SALib 2.0: advancing the accessibility and interpretability of global sensitivity analyses. SESMO 4, 18155. https://doi.org/10.18174/sesmo.18155.

Kummer, A., Varga, T., 2021. What do we know already about reactor runaway? – a review. Process Saf. Environ. Protect. 147, 460–476. https://doi.org/10.1016/j.psep.2020.09.059.

Lê, H.Q., Pokki, J.-P., Borrega, M., Uusi-Kyyny, P., Alopaeus, V., Sixta, H., 2018. Chemical recovery of gamma-valerolactone/water biorefinery. Ind. Eng. Chem. Res. 57, 15147–15158. https://doi.org/10.1021/acs.iecr.8b03723.

Leveneur, S., Vernieres-Hassimi, L., Salmi, T., 2016. Mass & energy balances coupling in chemical reactors for a better understanding of thermal safety. Educ. Chem. Eng. 16, 17–28. https://doi.org/10.1016/j.ece.2016.06.002.

Li, G., Lu, Z., Li, L., Ren, B., 2016. Aleatory and epistemic uncertainties analysis based on non-probabilistic reliability and its kriging solution. Appl. Math. Model. 40, 5703–5716. https://doi.org/10.1016/j.apm.2016.01.017.

Liu, X., Yin, L., Hu, L., Zhang, Z., 2017. An efficient reliability analysis approach for structure based on probability and probability box models. Struct. Multidiscip. Optim. 56, 167–181. https://doi.org/10.1007/s00158-017-1659-7.

Lyagoubi, N., Vernieres-Hassimi, L., Khalij, L., Estel, L., 2022. Quantification of the chemical reactor reliability in the presence of uncertainties/errors in input parameters. J. Loss Prev. Process. Ind. 76, 104751 https://doi.org/10.1016/j.jlp.2022.104751.

Martinez, A., Vernieres-Hassimi, L., Abdelouahed, L., Taouk, B., Mohabeer, C., Estel, L., 2022. Modelling of an anaerobic digester: identification of the main parameters influencing the production of methane using the Sobol method. Fuel 3, 436–448. https://doi.org/10.3390/fuels3030027.

Mohammadi, S., Cremaschi, S., 2022. Efficiency of uncertainty propagation methods for moment estimation of uncertain model outputs. Comput. Chem. Eng. 166, 107954 https://doi.org/10.1016/j.compchemeng.2022.107954.

Nannapaneni, S., Mahadevan, S., 2016. Reliability analysis under epistemic uncertainty. Reliab. Eng. Syst. Saf. 155, 9–20. https://doi.org/10.1016/j.ress.2016.06.005.

Pan, Y., Ren, C., Wang, G., Wang, Y., Zhang, X., Jiang, J., Shu, C.-M., 2023. Thermal hazard evaluation for gamma-valerolactone production by using formic acid as hydrogen donor. J. Loss Prev. Process. Ind. 81, 104951 https://doi.org/10.1016/j.jlp.2022.104951.

Salcedo, W.N.V., Mignot, M., Renou, B., Leveneur, S., 2023. Assessment of kinetic models for the production of gamma-valerolactone developed in isothermal, adiabatic and isoperibolic conditions. Fuel 350, 128792. https://doi.org/10.1016/j.fuel.2023.128792.

Shi, L., Delgado, J., Aoues, Y., Leveneur, S., 2023. Thermal risk assessment with mixed uncertainty propagation in gamma-valerolactone production. In: 2023 7th International Conference on System Reliability and Safety (ICSRS). IEEE, Bologna, Italy, pp. 350–354. https://doi.org/10.1109/ICSRS59833.2023.10381043.

Stoessel, F., 2020. Thermal Safety of Chemical Processes: Risk Assessment and Process Design, first ed. Wiley. https://doi.org/10.1002/9783527696918.

Tang, H., Li, D., Li, J., Xue, S., 2017. Epistemic uncertainty quantification in metal fatigue crack growth analysis using evidence theory. Int. J. Fatig. 99, 163–174. https://doi.org/10.1016/j.ijfatigue.2017.03.004.

Tsvetkova, O., Ouarda, T.B.M.J., 2021. A review of sensitivity analysis practices in wind resource assessment. Energy Convers. Manag. 238, 114112 https://doi.org/10.1016/j.enconman.2021.114112.

Tursi, A., 2019. A review on biomass: importance, chemistry, classification, and conversion. Biofuel Res. J. 6, 962–979. https://doi.org/10.18331/BRJ2019.6.2.3.

Virtanen, P., Gommers, R., Oliphant, T.E., Haberland, M., Reddy, T., 2020. SciPy 1.0: fundamental algorithms for scientific computing in Python. Nat. Methods 17, 261–272. https://doi.org/10.1038/s41592-019-0686-2.

Wang, Y., Cipolletta, M., Vernières-Hassimi, L., Casson-Moreno, V., Leveneur, S., 2019. Application of the concept of Linear Free Energy Relationships to the hydrogenation of levulinic acid and its corresponding esters. Chem. Eng. J. 374, 822–831. https://doi.org/10.1016/j.cej.2019.05.218.

Wang, Y., Plazl, I., Vernières-Hassimi, L., Leveneur, S., 2020. From calorimetry to thermal risk assessment: gamma-Valerolactone production from the hydrogenation of alkyl levulinates. Process Saf. Environ. Protect. 144, 32–41. https://doi.org/10.1016/j.psep.2020.07.017.

Yan, K., Yang, Y., Chai, J., Lu, Y., 2015. Catalytic reactions of gamma-valerolactone: a platform to fuels and value-added chemicals. Appl. Catal. B Environ. 179, 292–304. https://doi.org/10.1016/j.apcatb.2015.04.030.

Zhang, J., Xiao, M., Gao, L., Fu, J., 2018. A novel projection outline based active learning method and its combination with Kriging metamodel for hybrid reliability analysis with random and interval variables. Comput. Methods Appl. Mech. Eng. 341, 32–52. https://doi.org/10.1016/j.cma.2018.06.032.